CHEMISTRY OF MATERIALS

pubs.acs.org/cm

Article

Local Structure and Surface Acidity of Overlayers Prepared by Atomic Layer Deposition of Silica on Alumina

Melis Yarar, Zixuan Chen, Diana Piankova, Matthias Becker, Alexander V. Yakimov, Christophe Copéret, Pierre Florian,* Christoph R. Müller,* and Alexey Fedorov*

Cite This: *Chem. Mater.* 2025, 37, 7974–7986

Read Online

ABSTRACT: Understanding the structure of the silica−alumina interface and the reactivity of such interfacial sites in amorphous aluminosilicate (ASA) materials is essential due to their industrial utilization as solid acid catalysts. Here, we link the structure of silica layers grown on alumina by atomic layer deposition (ALD) to the acidic and catalytic properties of ASA. In particular, we study the local structure of silica overlayers as a function of the number of ALD cycles applied and reveal how the coordination environment of Al and Si sites governs the Lewis and Brønsted acidity and catalytic activity using methanol dehydration as a model structure-sensitive reaction. Relying on advanced solid-state NMR characterization, including ^{27}Al{^{29}Si} dipolar heteronuclear multiple-quantum coherence (D-HMQC) and ^{29}Si{^{27}Al} dipolar-mediated refocused insensitive nuclei enhanced by polarization transfer (D-RINEPT) experiments, dynamic nuclear polarization surface-enhanced NMR spectroscopy (DNP SENS), and infrared spectroscopy using probe molecules (CO, pyridine), we demonstrate that the atomic-scale mixing of silica and alumina generates strong Brønsted acidity and increases the strength of the Lewis acid sites. Our findings indicate that the density of acid sites is closely related to the coverage of the alumina surface by silica and can be controlled by the number of ALD cycles applied. This study advances our understanding of the relationship between the local environment of Si and Al sites, the abundance and strength of acid sites, and the superior high-temperature selectivity of SiO_x-Al_2O_3-based catalysts in methanol dehydration when compared to unmodified alumina.

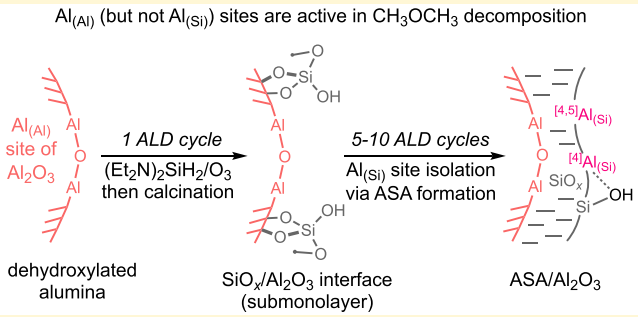

■ INTRODUCTION

Amorphous silica−alumina (ASA) materials are widely utilized in heterogeneous catalysis owing to the tunable strength and abundance of their Brønsted and Lewis acid sites (BAS and LAS, respectively).[1] Combined with a high specific surface area, the acidic properties of ASAs foster their catalytic applications in petrochemistry, biomass conversions, and fine chemicals, to name just a few.[1,2] Notably, the local coordination environment of Si and Al sites in ASA governs their surface acidity properties.[3,4] For example, Lewis acidity in ASA is associated with Al^{3+} sites, which can be tri-, tetra-, and pentacoordinate ($^{[3]}Al^{3+}$, $^{[4]}Al^{3+}$, and $^{[5]}Al^{3+}$, respectively).[3,5−7] Generally, the LAS strength depends on the coordination number of Al^{3+}; viz., sites on dehydroxylated alumina with a lower coordination number provide stronger LAS.[8−10] While $^{[3]}Al_{(Si)}{}^{3+}$ sites (such as $(\equiv SiO)_3Al$) sites) have not been unequivocally characterized in ASA materials, such sites are expected to be strong LAS.[11,12] $^{[4]}Al^{3+}$ sites in ASA can be strong or medium LAS; in contrast, $^{[5]}Al^{3+}$ sites have been associated with weaker LAS.[4,6,13,14] Similarly, the emergence and strength of BAS in ASAs depend on the local coordination environment of the silanol (Si−OH) and Al^{3+} sites,[15] which necessitates a proximity of the interacting sites, as found in pseudobridging $Al^{3+}\cdots(\mu^2-OH)-Si$ silanols (strong BAS).[12,15−18] The coordination geometry of Al sites in strong BAS has been proposed to be $^{[4]}Al^{3+}$.[13] Alternatively, pseudobridging silanols coordinated to a $^{[5]}Al^{3+}$ site or two neighboring $^{[4]}Al^{3+}$ and $^{[5]}Al^{3+}$ sites interacting with the same silanol have also been suggested to yield strong BAS.[19−22] Yet, the dependence of acid properties of ASA on the structure of the second coordination shell of the Al^{3+} sites, i.e., the relative ratio of Si and Al atoms and coordination number of Al atoms in $^{[n]}Al^{3+}{}_{(Si/Al)}$ (n = 4, 5, 6), is understood (and therefore controlled) to a lesser extent.[23,24]

Disentangling complex local structures, such as those in ASA, has been greatly aided by element-specific magic angle spinning nuclear magnetic resonance spectroscopy (MAS

Received: July 11, 2025
Revised: September 22, 2025
Accepted: September 23, 2025
Published: September 30, 2025

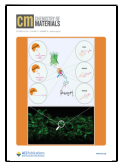

https://doi.org/10.1021/acs.chemmater.5c01832
Chem. Mater. 2025, 37, 7974−7986

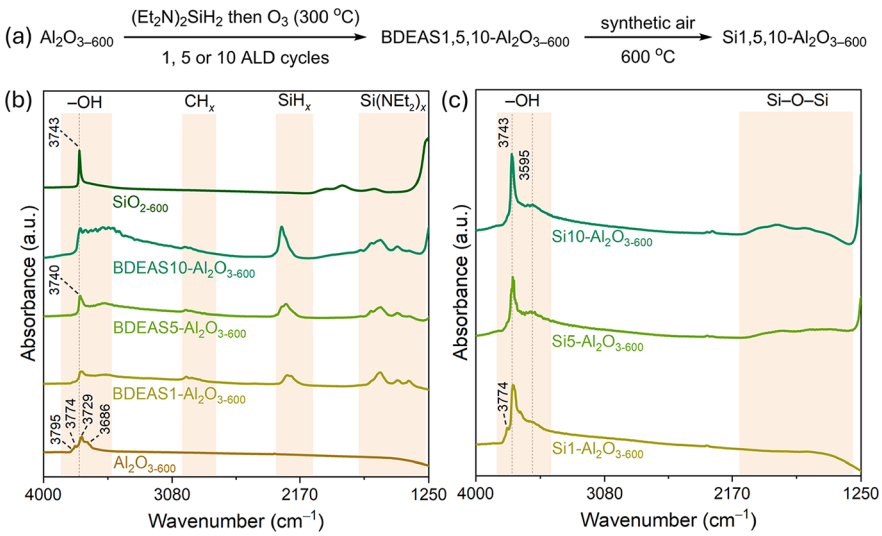

Figure 1. (a) Synthetic approach to obtain the Si−Al_2O_3 materials studied in this work; transmission FTIR spectra of (b) Al_2O_{3-600}, BDEAS1,5,10-Al_2O_{3-600}, and SiO_{2-600} and (c) Si1-, Si5, and Si10−Al_2O_{3-600}.

NMR).[25−28] In addition to the insights discussed above, advanced two-dimensional NMR at an ultrahigh magnetic field strength (35.2 T) has revealed that pseudobridging silanols in ASA coexist with distinct strong BAS, similar to Si−OH−Al sites in zeolites.[28,29] Dynamic nuclear polarization surface enhanced NMR spectroscopy (DNP SENS) provides additional structural information about surface sites due to sensitivity enhancement.[30,31] For instance, results of a recent DNP SENS study suggested that a $^{[4]}Al^{3+}\cdots(\mu^2-OH)-Si$ connectivity accounts for the main pseudobridging silanol structure.[25] Surface acidity properties are typically assessed by NH_3 temperature-programmed desorption experiments or Fourier transform infrared spectroscopy studies using basic probe molecules, such as pyridine (Py-FTIR).[27] However, the complementary use of ^{15}N-labeled pyridine (Py) allows the extraction of detailed acidity information from ^{15}N DNP SENS spectra because this method is particularly sensitive to BAS.[32] This sensitivity is attributed to the direct N−H bond in the pyridinium cation, which provides enhanced NMR signal intensity.[33] In addition, ^{15}N DNP SENS experiments are performed at a low temperature, allowing surface diffusion to be slowed down; for instance, ^{15}N DNP SENS allowed the resolution of two strong BAS in AlO_x/SiO_2 and GaO_x/SiO_2 materials.[24,34]

Given that surface acidity is a key property for the catalytic application of ASAs, controlling the strength and relative distribution of LAS and BAS is essential yet challenging.[5,35,36] In this context, atomic layer deposition (ALD) has emerged as a method of choice for tuning the surface properties of mixed oxides.[37−39] Here, the tuning of the strength and distribution of LAS and BAS relies on understanding the atomic-scale interaction between the support and the ALD precursor, which can be enhanced by utilizing a dehydroxylated, supporting oxide to favor grafting reactions in preference over hydrolysis of the ALD precursors by the physisorbed water.[24,34] The grafting reaction typically entails the interaction of alkyl or amide ligands of the ALD precursor with surface hydroxyls or oxo groups.[5,40] The deposition of AlO_x overlayers is one of the most studied ALD reactions.[41] In particular, we previously employed this approach to deposit trimethylaluminum on dehydroxylated silica, obtaining AlO_x overlayers after ozonolysis and calcination steps.[24] The first ALD cycle yields mostly tetra- and pentacoordinate Al sites with 3−4 and 2 Si atoms in the second coordination sphere, respectively, i.e., $^{[4]}Al_{(3-4Si)}$ and $^{[5]}Al_{(2Si)}$ sites. The resulting AlO_x-SiO_2 material displayed strong Brønsted acidity. However, consecutive ALD cycles led to the formation of amorphous alumina layers with a higher concentration of $^{[5]}Al_{(Al)}$ sites. Such AlO_x overlayers showed a decreased relative amount of strong BAS and increased relative amounts of LAS of lower strength relative to the ASA interphase formed when applying 1 ALD cycle.[24] Similar observations regarding the strength and abundance of acid sites with the number of applied ALD cycles were made for GaO_x overlayers on SiO_2.[34]

Here, we engineer model surfaces and interfaces by applying a varying number of ALD cycles (1, 5, or 10) of bis(diethylamino)silane onto dehydroxylated γ-Al_2O_3. By controlling the number of ALD cycles, we obtained three materials referred to as Si1-, Si5-, and Si10−Al_2O_3 with surface sites that differ in the relative strength and abundance of LAS and BAS. The local structure of the Al sites was refined through MAS NMR experiments, particularly ^{29}Si DNP SENS, ^{27}Al{^{29}Si} dipolar-mediated heteronuclear multiple-quantum coherence (D-HMQC) and ^{29}Si{^{27}Al} dipolar-mediated refocused insensitive nuclei enhanced by polarization transfer (D-RINEPT) with Carr−Purcell−Meiboom−Gill (CPMG) detection. These structural insights allowed us to rationalize the acidity properties of the prepared materials and their relevance for the catalytic dehydration of methanol to dimethyl ether. In stark contrast to the deposition of AlO_x on amorphous dehydroxylated silica, which features a decreasing BAS-to-LAS ratio with increasing ALD cycles,[24] this ratio first increases for up to approximately 5 ALD cycles when SiO_x is deposited onto dehydroxylated alumina and only then decreases. Another notable difference is the increasing strength of LAS with the number of ALD cycles applied. Comparing Al_2O_3 to Si1-, Si5-, and Si10−Al_2O_3 in methanol dehydration reveals that, at temperatures ≤350 °C, unmodified Al_2O_3 and Si1−Al_2O_3 exhibit higher space-time yields of dimethyl ether (DME) than Si5-, and Si10−Al_2O_3. However, Si5- and Si10−Al_2O_3 appreciably outperform Si1−Al_2O_3 and Al_2O_3 at 450 °C due to a higher DME selectivity and lower selectivity to

https://doi.org/10.1021/acs.chemmater.5c01832
Chem. Mater. 2025, 37, 7974−7986

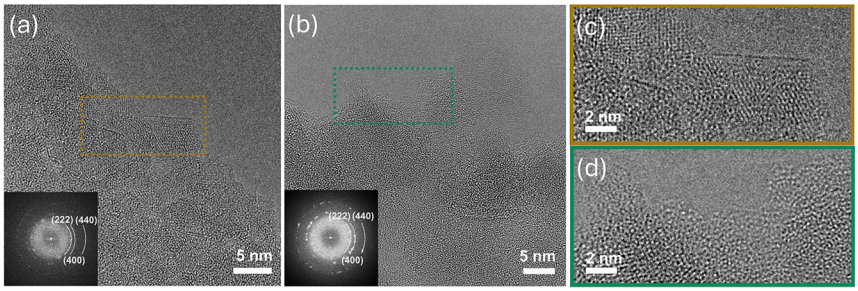

Figure 2. Overview HRTEM images of the surface of (a) Al_2O_{3-600} and (b) Si10−Al_2O_{3-600} with the corresponding FFT patterns indexed to γ-Al_2O_3 in insets. The panels (c, d) show HRTEM images magnified from (a) and (b), taken from the respective colored boxed areas.

methane. Thus, the deposition of SiO_x onto Al_2O_3 allows for the chemical blocking of the unselective $Al_{(Al)}$ sites of unmodified Al_2O_3.

■ EXPERIMENTAL SECTION

Materials and Methods. The three Si−Al_2O_3 materials studied in this work were synthesized by ALD at 300 °C using bis-(diethylamino)silane (BDEAS) as the ALD precursor, alumina (Puralox, SBa 200, Sasol) dehydroxylated at 600 °C (denoted Al_2O_{3-600}) as the support, and ozone as the oxidant between subsequent ALD cycles; see the Supporting Information file for further details. The number of ALD cycles performed was 1, 5, or 10, and the as-deposited materials are denoted BDEAS1-, BDEAS5-, and BDEAS10-Al_2O_{3-600}, respectively. Treating the as-deposited materials at 600 °C for 3 h under a flow of synthetic air (50 mL min^{-1}) yielded calcined materials denoted as Si1-, Si5-, and Si10−Al_2O_{3-600}. The calcined materials were handled without exposure to ambient air unless specified otherwise. The Supporting Information file contains details concerning the applied characterization methods, including inductively coupled plasma optical emission spectroscopy (ICP-OES), scanning/transmission electron microscopy (STEM and TEM), powder X-ray diffraction (XRD), N_2 physisorption, ammonia temperature-programmed desorption (NH_3-TPD), Py-FTIR, diffuse reflectance infrared Fourier transform spectroscopy with carbon monoxide used as the probe molecule (CO−DRIFTS), ^{15}N and ^{29}Si DNP SENS, and $^{27}Al\{^{29}Si\}$ D-HMQC and $^{29}Si\{^{27}Al\}$ D-RINEPT CPMG experiments. The catalytic activity in converting methanol to dimethyl ether was tested in a temperature range of 150−450 °C and at a space velocity of 2.90 h^{-1} using a Microactivity EFFI reactor (PID Eng&Tech). The progress of the reaction was probed by an online gas chromatograph (CompactGC 4.0, Gas Analyzer Solutions).

■ RESULTS

Synthesis of Si−Al_2O_3. The materials Si1-, Si5-, and Si10−Al_2O_3 were prepared using 1, 5, or 10 ALD cycles, with BDEAS as the precursor and Puralox alumina dehydroxylated at 600 °C as the support; the deposition temperature was 300 °C (Figure 1a). The self-limiting surface saturation conditions for one ALD cycle were mapped by determining the number of BDEAS pulses required to consume all reactive aluminol (Al−OH) FTIR bands. For instance, while 5 pulses of BDEAS led to only a partial disappearance of the isolated aluminol bands at ca. 3795, 3774, 3729, and 3686 cm^{-1},[5] 20 pulses of BDEAS resulted in a nearly complete disappearance of these bands (Figure S2). Hence, 20 pulses of BDEAS were considered sufficient to yield a surface saturation of the ALD precursor. The deposition of BDEAS is also evident from the appearance of characteristic CH_x, SiH_x, and $Si(NEt_2)_x$ bands at ca. 3050−2770 cm^{-1}, 2270 cm^{-1}, and 1780−1315 cm^{-1}, respectively (Figure 1b).[42] Ozonolysis at 300 °C, applied after the BDEAS pulses, largely restored the OH intensity, while simultaneously decreasing the intensity of the CH_x, SiH_x, and $Si(NEt_2)_x$ bands in BDEAS1-Al_2O_{3-600} (Figure S2). A calcination treatment at 600 °C was performed to remove the remaining precursor surface species in BDEAS1-, BDEAS5-, and BDEAS10-Al_2O_{3-600}, yielding the materials Si1-, Si5-, and Si10−Al_2O_{3-600} that do not feature any ALD precursor bands (Figure 1c). Consistent with the deposition of SiO_x onto Al_2O_{3-600}, FTIR spectra of Si5- and Si10−Al_2O_{3-600} reveal a growing intensity of Si−O−Si vibrations at ca. 2150−1250 cm^{-1}, which can, however, not be discerned in Si1−Al_2O_{3-600}. The intensity of the aluminol bands decreases with the number of ALD cycles applied, while in parallel, a band at 3743 cm^{-1} gradually appears, attributed to the formation of isolated silanols.[43] In addition, the band at ca. 3595 cm^{-1} increases in intensity with the number of applied ALD cycles; this band is attributed to Si−OH interacting with LAS (Figure 1c).

Basic Characterization. To assess the Si content, the crystalline phase(s), surface area, and porosity of the prepared materials, ICP-OES, XRD, and N_2 physisorption experiments were performed (after exposure to ambient air), respectively. ICP-OES determined that the Si weight fraction in Si1-, Si5-, and Si10−Al_2O_3 is 1.1, 5.9, and 9.9 wt %, respectively (Table S1). The surface area and pore volume evaluated by N_2 physisorption and determined using the Brunauer−Emmett−Teller (BET) and Barrett−Joyner−Halenda (BJH) models (Figures S3 and S4) are presented in Table S1. The BET surface area increases with the number of ALD cycles from 150 m^2 g^{-1} in Al_2O_{3-600} to 154, 169, and 168 m^2 g^{-1} for Si1-, Si5-, and Si10−Al_2O_{3-600}, which corresponds to 1.5, 8.3, and 13.7 Si nm^{-2}, respectively (Table S1). The increase of the surface area with an increasing amount of SiO_x deposited onto alumina is likely due to surface amorphization induced by the ALD of SiO_x onto initially crystalline γ-Al_2O_3, as elaborated further below. Yet the pore volume of Al_2O_{3-600} and Si1,5,10-Al_2O_{3-600} was very similar, i.e., ca. 0.4 cm^3 g^{-1}. XRD patterns of Si1-, Si5-, and Si10−Al_2O_3, along with the references Al_2O_3 and SiO_2, are given in Figure S5. The bulk structure of the alumina support, as probed by XRD, remained unchanged for all three prepared Si−Al_2O_3 materials (γ-Al_2O_3), i.e., no shifts in the peak positions were detected. Yet, for Si5- and Si10−Al_2O_{3-600}, a halo centered around a 2θ value of 21° that is attributed to amorphous SiO_2 of the deposited silica layers was observed.

Further, using energy-dispersive X-ray spectroscopy (EDX) maps, we observed a homogeneous distribution of Si on the air-exposed Si1-, Si5-, and Si10−Al_2O_{3-600} (Figure S6). To gain insight into the morphology of the deposited SiO_x layers at the nanoscale, we compared the initial material Al_2O_{3-600} to Si10−Al_2O_{3-600} using high-resolution transmission electron microscopy (HRTEM). Al_2O_{3-600} contains particles with

https://doi.org/10.1021/acs.chemmater.5c01832
Chem. Mater. 2025, 37, 7974−7986

diameters of 1−2 μm, comprised of smaller, aggregated crystallites of approximately tens of nanometers in size (Figure 2a). However, Si10−Al_2O_{3-600} features a significantly modified morphology relative to Al_2O_{3-600} (Figure 2b). Specifically, despite the poor crystallinity of the crystallites in Al_2O_{3-600}, their surface is well-defined (Figure 2c). In contrast, on Si10−Al_2O_{3-600}, an amorphous surface layer of several nanometers in thickness is observed on the γ-Al_2O_3 crystallites (Figure 2b,d, overview in Figure S7), suggesting that the surface layer is very likely comprised of SiO_x, i.e., there is no TEM-detectable surface exposure of the Al_2O_3 support. Such a core−shell microstructure is consistent with EDX line-scan analysis, which shows a higher Si intensity at (or close to) the surface (Figure S8).

Methanol-to-DME Catalytic Tests. The catalytic performance of our Si−Al_2O_{3-600} materials in the dehydration of methanol, i.e., methanol-to-dimethyl ether conversion, was evaluated by passing a flow of 0.75% CH_3OH/N_2 through a catalyst bed in the temperature range of 150−450 °C, with temperature increments of 100 °C. Using a weight hour space velocity (WHSV) of 2.90 h^{-1}, the methanol conversion and product formation rate were monitored by GC for a duration of 70 min at each tested temperature. The catalytic results are summarized in Figure 3 and Table S3. At 150 °C, the methanol conversion was below 1.5% for all three Si−Al_2O_{3-600} materials and the Al_2O_{3-600} and SiO_{2-600} references. At 250 °C, the methanol conversion decreased with increasing Si loading, specifically from 76.4% for Al_2O_{3-600} to 70.2, 37.3, and 25.1% for Si1-, Si5-, and Si10−Al_2O_{3-600}, respectively (Figure 3a). All catalysts exhibited a 100% selectivity toward DME (Table S3).

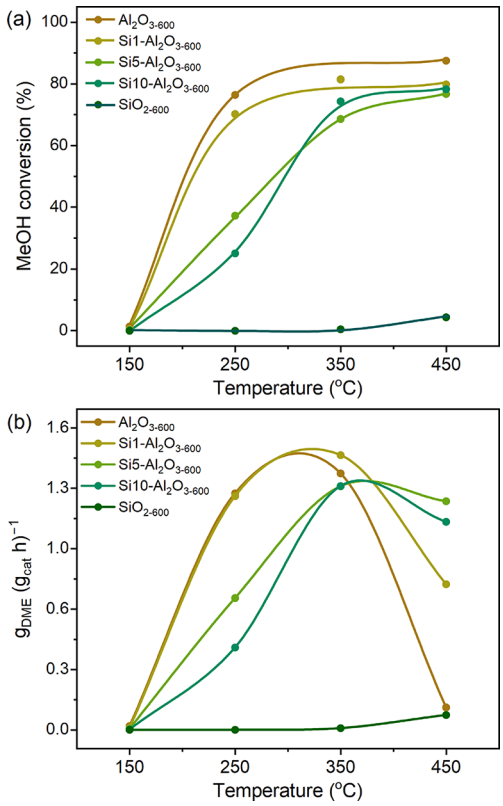

Figure 3. (a) Methanol conversion and (b) space-time yield of DME as a function of temperature under methanol dehydration conditions; the trendlines are added to guide the eye.

Generally, the methanol conversion increased with temperature while the difference between the catalysts diminished such that at 450 °C, all of the Si−Al_2O_{3-600} materials and Al_2O_{3-600} displayed a methanol conversion close to the equilibrium conversion (ca. 80%),[44] while SiO_{2-600} remained almost inactive.

However, for all four catalysts, the space-time yield of DME (STY_{DME}) at 450 °C is lower than at 350 °C (Figure 3b). The decrease in STY at 450 °C is most pronounced for Al_2O_{3-600} and, to a lesser extent, for Si1−Al_2O_{3-600}, which show a STY_{DME} of 1.36 and 1.46 g_{DME} $(g_{cat}\ h)^{-1}$ at 350 °C that decrease to 0.119 and 0.772 g_{DME} $(g_{cat}\ h)^{-1}$ at 450 °C, respectively. For Si5- and Si10−Al_2O_{3-600}, the decrease in STY_{DME} is more modest, i.e., from 1.29 and 1.29 g_{DME} $(g_{cat}\ h)^{-1}$ at 350 °C to 1.21 and 1.10 g_{DME} $(g_{cat}\ h)^{-1}$ at 450 °C, respectively. The lower STY_{DME} at 450 °C parallels a decreasing selectivity for DME due to the formation of CH_4 (Figure S9). In this context, the decomposition of DME to CH_4, H_2, and CO has been reported above 350 °C on Al_2O_3.[44,45] Notably, we did not detect CO in our experiments, indicating that its concentration in the effluent gas is <500 ppm (the detection limit of CO by the GC used). Additionally, in all experiments, the carbon balance is in the range of 80−90%. All postreaction catalysts are gray, suggesting no appreciable coke deposition. Indeed, we did not observe Raman bands due to carbon in postreaction alumina (analyzed as a representative catalyst, Figure S16a). Attenuated total reflectance infrared spectrum of the postreaction alumina presented in Figure S16b displays an intense band at 1046 cm^{-1} and a weak band at 1578 cm^{-1}, likely due to C−O and C═O vibrations, respectively, and no bands in the C−H regions. As the bands at 1046 and 1578 cm^{-1} are not observed on fresh alumina (exposed to air, Figure S16b), these are assigned to oxygenates such as carbonates or oxalates.[44−47] Therefore, the low carbon balance is likely due to the formation of oxygenates that remain adsorbed on the surface of the catalysts at the explored reaction temperatures or cannot be quantified reliably by the employed GC method.[45] Lastly, we note that while the catalytic tests discussed above were performed with catalysts loaded into reactors in air, a control experiment reveals similar catalytic performance for Al_2O_{3-600} loaded in air and in pristine conditions (glovebox handling, see Table S3). As the adsorption energy of the reaction intermediates and products depends on the strength of the acid sites, in the following, we assess how the surface acidity changes with the thickness of the silica overlayer (controlled by the number of ALD cycles) and relate surface acidity to the local structure of the interacting Si and Al sites.

Surface Acidity. Experiments using the basic probe molecules ammonia and pyridine were employed to investigate the surface acidity of the prepared materials.[48] First, the total number of acid sites was quantified via NH_3 TPD studies. Here, the air-exposed catalysts were pretreated in a flow of Ar at 600 °C, cooled down to 120 °C, and the dehydroxylated materials were exposed to a flow of 5% NH_3/He for 30 min. NH_3 desorption profiles were obtained during heating of the materials to 600 °C in a He flow (20 mL min^{-1}) with a heating ramp of 10 °C min^{-1}. The MS signal at m/z = 16 was used for quantification to prevent a possible contribution from water fragmentation.[49] Figure 4a shows that on Al_2O_{3-600}, the peak in the NH_3 desorption profile is centered around 250 °C. The desorption profiles for the Si−Al_2O_3 materials showed a broadening, and the intensity of the NH_3 desorption peak

https://doi.org/10.1021/acs.chemmater.5c01832
Chem. Mater. 2025, 37, 7974−7986

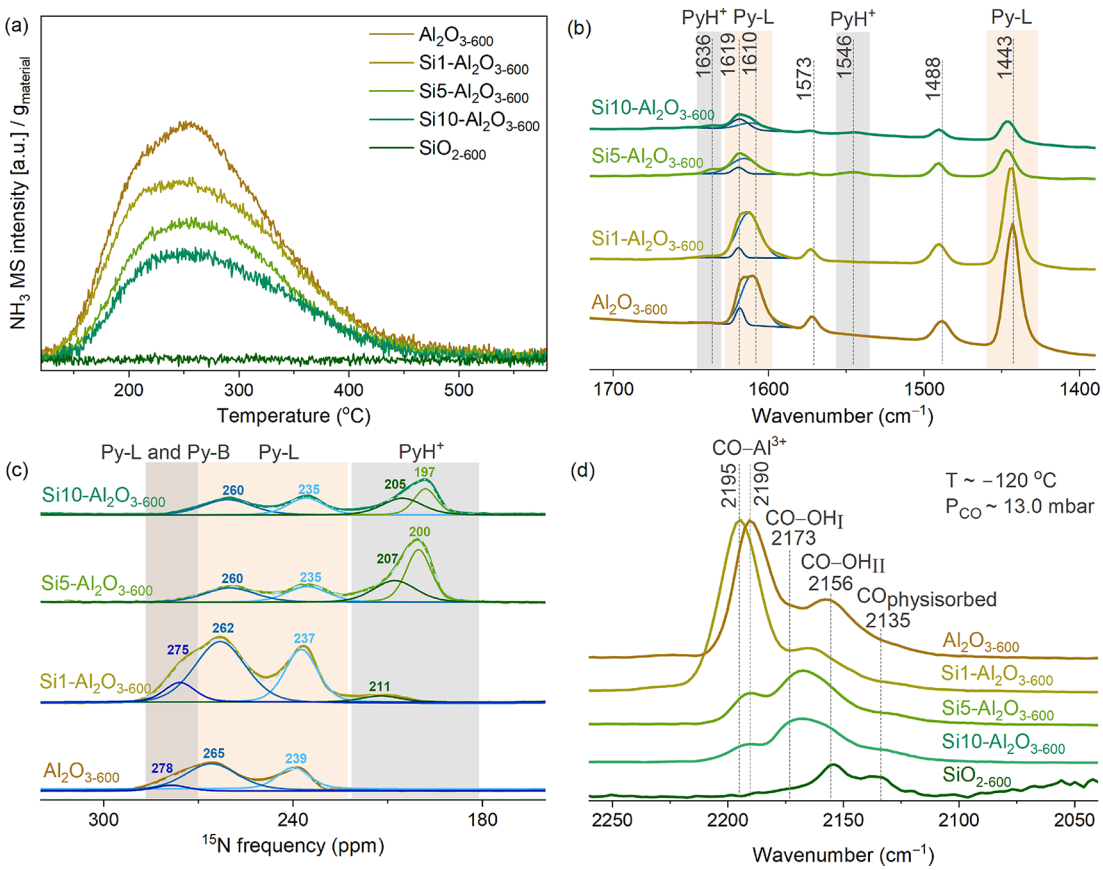

Figure 4. NH_3 TPD profiles (a), Py-FTIR (b), ^{15}N DNP SENS (c), and CO−DRIFTS (d) spectra of Al_2O_{3-600}, Si1-, Si5-, Si10−Al_2O_{3-600}, and SiO_{2-600}. In (b) and (c), ^{15}N-Py was desorbed at 150 °C. PyH^+, Py−L, and Py−B indicate protonated pyridine and pyridine interacting with LAS and weak BAS, respectively. The spectra in (d) were obtained under ca. 13 mbar of CO at −120 °C.

gradually decreased with increasing Si content. There was no NH_3 desorption from SiO_{2-600}. This trend suggests a reduction in the total amount of surface acid sites with increasing Si loading, consistent with previous reports on Si deposition onto alumina.[14] Quantifying the amount of NH_3 desorbed, Table S4 demonstrates that 316 μmol of NH_3 desorbed from one gram of Al_2O_{3-600}, corresponding to 1.26 NH_3 molecules per nm^2, which is comparable to the value reported previously for Puralox γ-Al_2O_3 pretreated at 550 °C (350 μmol g^{-1}, 1.04 NH_3 molecules per nm^2).[50] The amount of NH_3 desorbed decreased to 259, 202, and 157 μmol g^{-1} for Si1-, Si5-, and Si10−Al_2O_{3-600}, respectively. The desorption profiles were deconvoluted using three components for Al_2O_{3-600} and Si1−Al_2O_{3-600} and two components for Si5−Al_2O_{3-600} and Si10−Al_2O_{3-600} (Figure S11). However, such a deconvolution does not allow the separation of the NH_3 desorption peaks into LAS and BAS.

To allow for a discrimination of LAS and BAS, transmission FTIR and ^{15}N DNP SENS experiments using pyridine as the probe molecule were used. Toward this end, dehydroxylated Al_2O_{3-600}, Si−Al_2O_{3-600}, and SiO_{2-600} were exposed to a vapor of ^{15}N-Py at room temperature, followed by outgassing for 1 h at 150 °C and ca. 10^{-5} mbar. The bands due to Py adsorbed on LAS (Py-L) were observed in the regions 1460−1420 and 1630−1600 cm^{-1} (Figure 4b).[51] Al_2O_{3-600} features a broad band in the range 1630−1600 cm^{-1} that can be deconvoluted into two peaks centered at 1619 cm^{-1} and 1610 cm^{-1} (due to Py adsorbed on stronger and weaker LAS, minor and major contributions, respectively). With increasing Si loading, the contribution from the peak at 1610 cm^{-1} decreased gradually. For Si1−Al_2O_{3-600}, the band at 1610 cm^{-1} shifted to ca. 1615 cm^{-1}, indicating that the deposition of a submonolayer SiO_x increased the strength of weak/medium alumina-based LAS. At the same time, the relative intensity of the band at 1619 cm^{-1} decreased in Si1−Al_2O_{3-600} compared to Al_2O_{3-600}, consistent with the deposition of SiO_x onto strong LAS of Al_2O_{3-600}. For Si10−Al_2O_{3-600}, the contribution from the peak at 1619 cm^{-1} to the overall Py-L signal dominates. This observation suggests an increasing relative ratio of stronger to weaker LAS with increasing Si loading. Another clear trend is the decreasing intensity of the bands due to Py adsorbed on LAS (seen in both regions mentioned above) with increasing Si loading, a consequence of the covering of Al^{3+} sites by SiO_x. No appreciable amount of Py was observed on SiO_{2-600} under the conditions employed (Figure S12). The bands of pyridinium (PyH^+) at 1546 cm^{-1} and 1636 cm^{-1} were discerned for Si5- and Si10−Al_2O_{3-600}, indicating the emergence of strong Brønsted acidity in these two materials; such bands were absent in Si1−Al_2O_{3-600} and Al_2O_{3-600}.[51] This trend is opposite to the one observed when layers of AlO_x were deposited onto SiO_2 by ALD.[24]

The number of LAS in our materials can be estimated from the acquired Py-FTIR spectra utilizing the Beer−Lambert-Bouguer law using a reported molar absorption coefficient for Py on LAS (ε_{Py-L}) of 1.87 cm μmol^{-1}.[52,53] For this analysis, we used unlabeled Py (see the SI file for details and Figure S12) and obtained 130 μmol g^{-1} of Py adsorbed on LAS in Al_2O_{3-600}, in agreement with the reported value of 125 μmol

https://doi.org/10.1021/acs.chemmater.5c01832
Chem. Mater. 2025, 37, 7974−7986

g^{-1} for γ-Al_2O_3 dehydroxylated at 450 °C.[53] The amount of LAS on Si1−Al_2O_{3-600} was similar to that of Al_2O_{3-600}, i.e. 135 μmol g^{-1} but decreased to 68 and 51 μmol g^{-1} for Si5- and Si10−Al_2O_{3-600}, respectively (Table S4). We limit the FTIR-based quantification to the Lewis acid sites as the extinction coefficient for PyH^+ on ASA has not been reported, and the extinction coefficient for PyH^+ on zeolites has been reported to depend on the zeolite structure, hindering an appropriate selection.[53]

The evolution of the strength of the LAS and BAS with increasing number of Si ALD layers was further refined through ^{15}N DNP SENS experiments; the spectra and the peak fitting results are presented in Figure 4c and Table S5. The spectrum of Al_2O_{3-600} shows peaks at ^{15}N chemical shifts of 278, 265, and 239 ppm, consistent with previous observations for Al_2O_{3-500}.[54] The peaks at 239 and 265 ppm are due to strong and medium strength LAS, respectively, while the minor peak at 278 ppm is due to Py adsorbed on either weak LAS or BAS.[54−58] Si1−Al_2O_{3-600} displayed more shielded signals, i.e., shifted to 275, 262, and 237 ppm. In addition to the peak shift, the relative intensity of the peak at 275 ppm increased, and a low-intensity peak due to PyH^+ appeared at 211 ppm. The strength of the medium and strong LAS further increased in Si5- and Si10−Al_2O_{3-600}; viz., the peaks due to Py-L were further shifted to 260 and 235 ppm. The least shielded peak at 278−275 ppm disappeared for Si5- and Si10−Al_2O_{3-600}, while peaks due to two strong BAS appeared, i.e., two PyH^+ peaks at 207 and 200 ppm for Si5- and at 205 and 197 ppm for Si10−Al_2O_{3-600}, respectively. Similarly, two strong BAS were reported for ALD-prepared Al-SiO_{2-500} and Ga-SiO_{2-500} materials.[24,34]

Lastly, CO−DRIFTS studies were utilized to refine changes in weak BAS and LAS with increasing Si content.[13] In such experiments, the materials were dehydroxylated in a Harrick cell at 600 °C at ca. 10^{-4} mbar overnight; subsequently, CO was admitted to the cell at −120 °C in increments of 7 mbar until a CO partial pressure of ca. 100 mbar was achieved. The complete CO adsorption and desorption profiles are presented in Figures S13 and S14, while the profiles obtained at ca. 13 mbar CO pressure during CO adsorption are plotted in Figure 4d. Al_2O_{3-600} featured an intense band at 2190 cm^{-1} corresponding to CO interacting with Al^{3+} sites.[59,60] This band was blue-shifted to 2195 cm^{-1} in Si1−Al_2O_{3-600} and to 2193 cm^{-1} in both Si5- and Si10−Al_2O_{3-600}. These wavenumbers are within the typical range of CO−Al^{3+} adducts on alumina (2190−2230 cm^{-1}).[13,27,61] It was reported that isolated Al^{3+} sites, such as corner or edge Al^{3+} sites of alumina or dispersed (isolated) Al^{3+} sites on ASA, form adducts at higher CO frequencies (ca. 2230−2215 cm^{-1}) compared to bulk or higher coordinated Al^{3+} sites (2190−2196 cm^{-1}).[61,62] Based on these assignments, the observed shift to higher wavenumbers after Si deposition can be interpreted as an increase in the strength of LAS, which is associated with a decrease in the coordination number and isolation of Al^{3+} sites. With increasing number of ALD cycles, the intensity of the CO−Al^{3+} band reduced appreciably, in particular when comparing Al_2O_{3-600} and Si1−Al_2O_{3-600} to Si5- and Si10−Al_2O_{3-600}. The decreasing intensity of the CO−Al^{3+} band with increasing quantity of Si deposited is linked to the covering of Al^{3+} LAS with SiO_x, consistent with the NH_3 TPD, Py-FTIR, and ^{15}N-Py-DNP SENS results discussed above. The presence of weak BAS on Al_2O_{3-600}, i.e., OH groups interacting with CO, was identified by a band centered at 2156 cm^{-1};[63] this band was also observed on SiO_{2-600}. On Si1-, Si5-, and Si10−Al_2O_{3-600}, a new band at, respectively, 2162, 2168, and 2173 cm^{-1} appeared. This band is ascribed to CO interacting with strong BAS.[63,64] The shift to higher wavenumbers of this band indicates an increasing strength of BAS. These results confirm that the amount and strength of strong BAS increases with increasing number of Si ALD cycles and that the acidic strength of LAS on Al_2O_{3-600} increases with Si deposition, while the amount of LAS decreases.

Local Environment of Si. To assess the structure of Si atoms in Si1-, Si5-, and Si10−Al_2O_{3-600}, ^{29}Si DNP SENS experiments using a contact time of 2 ms were performed. The resulting spectra and corresponding fittings are presented in Figure 5. The fitting results are compiled in Table S2. In general, three components were sufficient to fit all spectra. While the Si sites in Si5−Al_2O_{3-600} and Si10−Al_2O_{3-600} are qualitatively similar, the spectrum of Si1−Al_2O_{3-600} is appreciably different. For Si1−Al_2O_{3-600}, the most intense peak is at a chemical shift of −82.6 ppm, while the less intense peaks are located at −89.1 and −92.8 ppm. Already for Si5−Al_2O_{3-600}, the peak at −85.9 ppm becomes a minor peak relative to the peaks centered at −92.4 and −99.9 ppm. The relative intensity of the peaks and their chemical shifts further evolve for Si10−Al_2O_{3-600} such that the peak at −101.6 ppm is the most prominent, followed by the peak at −93.1 ppm and a low-intensity peak at −86.2 ppm. The more deshielded peak in Si1−Al_2O_{3-600} is attributed to Si species with an increasing number of Al atoms in the second coordination sphere (such as $Si_{(3-4Al)}$) and/or carrying OH groups.[65] The higher degree of shielding for an increasing Si content (i.e., lower chemical shifts) suggests an increasing polymerization of the silica network incorporating fewer aluminum atoms.[66]

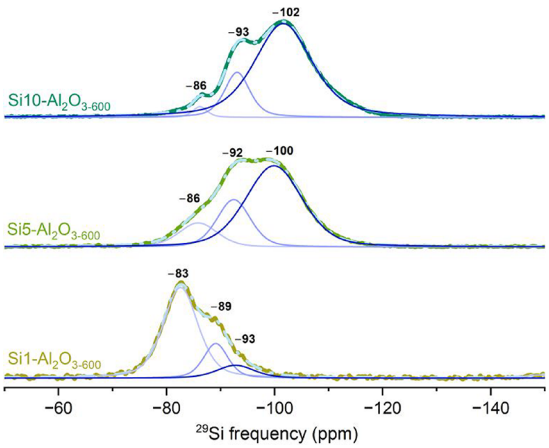

Figure 5. ^{29}Si DNP SENS data of Si1-, Si5-, and Si10−Al_2O_{3-600}. The simulation is presented as a dashed light-blue trace, with the individual fitted components shown as solid blue traces.

Si−O−Al Connectivity. Figure 6a,b displays the spectra obtained for Si1- and Si10−Al_2O_{3-600} using one-dimensional $^{27}Al\{^{29}Si\}$ D-HMQC experiments at varying recoupling times, which allowed probing Al species at various distances from Si sites, since increasing the dipolar-based recoupling time extends the distances at which recoupling occurs.[67] At a short recoupling time of 1.5 ms, these ^{29}Si-filtered ^{27}Al spectra mainly provide information about the SiO_x/Al_2O_3 interface, i.e., Al atoms close to Si contribute primarily to the signal. Note that the sites of the SiO_x/Al_2O_3 interface reside at the

https://doi.org/10.1021/acs.chemmater.5c01832
Chem. Mater. 2025, 37, 7974−7986

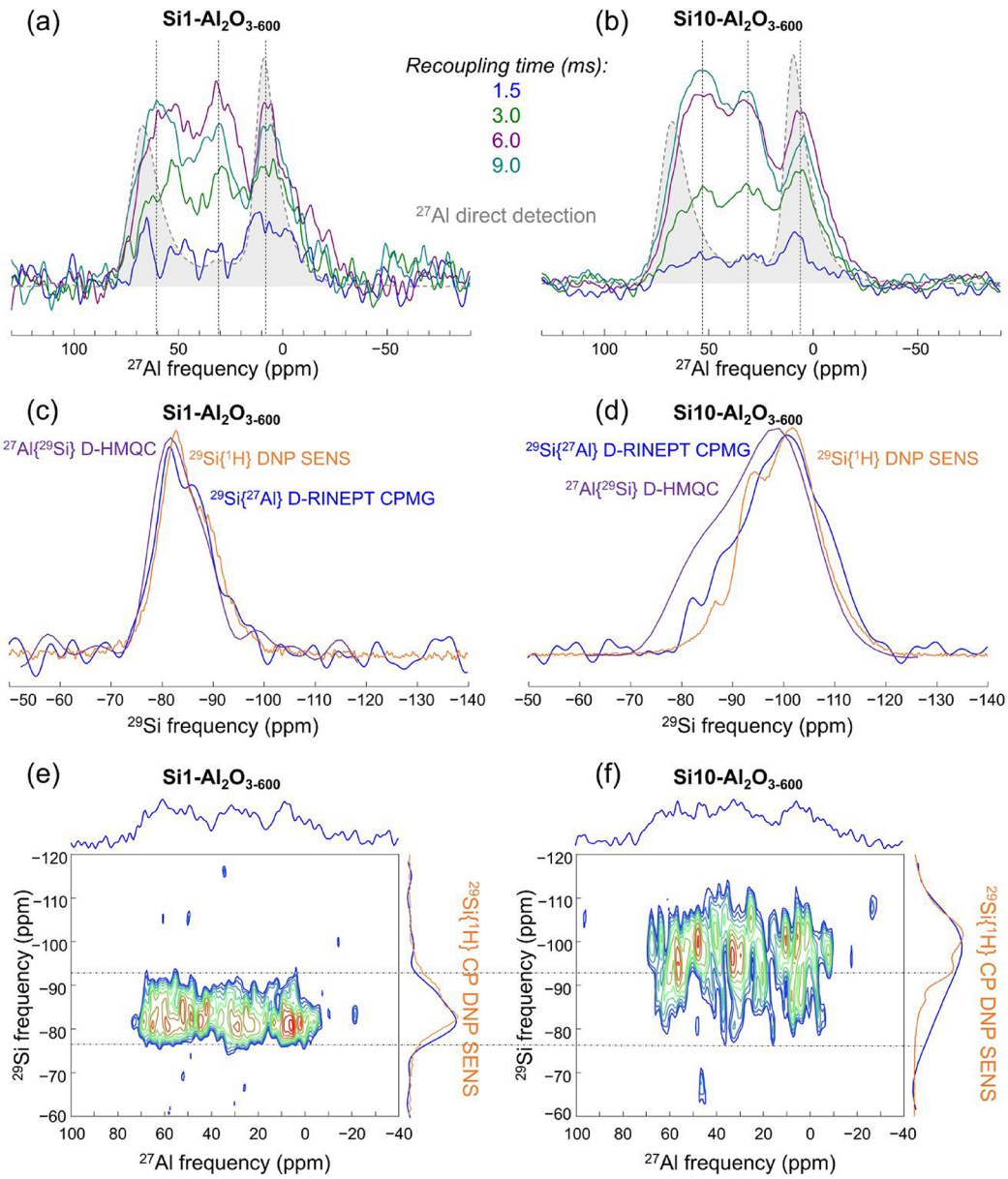

Figure 6. ^{27}Al{^{29}Si} SR4$^2_1$ D-HMQC spectra of (a) Si1−Al_2O_{3-600} and (b) Si10−Al_2O_{3-600} at 17.6 T using various recoupling times; for the 6.0 ms experiment, the S/N is 7.6 for Si1−Al_2O_{3-600} and 10.6 for Si10−Al_2O_{3-600}. Direct detection ^{27}Al spectrum of the Al_2O_3 reference is given in gray, and the dashed vertical lines are a guide for the eyes to indicate the position of the $^{[4]}$Al, $^{[5]}$Al, and $^{[6]}$Al sites, respectively. A comparison of ^{29}Si{^{27}Al} SR4$^2_1$ D-RINEPT CPMG, ^{29}Si{^{1}H} DNP SENS, and the ^{29}Si projection of the 2D ^{27}Al{^{29}Si} SR4$^2_1$ D-HMQC spectra (blue, orange, and purple, respectively) of (c) Si1−Al_2O_{3-600} and (d) Si10−Al_2O_{3-600}. ^{27}Al{^{29}Si} SR4$^2_1$ D-HMQC 2D correlation spectra of (e) Si1−Al_2O_{3-600} and (f) Si10−Al_2O_{3-600} obtained with a recoupling time of 6.0 ms. ^{29}Si{^{1}H} DNP SENS spectra are shown in orange in the vertical projections. Horizontal dashed lines guide the eye to locate the maxima in the ^{29}Si dimension.

outer surface and subsurface for Si1- and Si10−Al_2O_{3-600}, respectively. Experiments with a prolonged recoupling time, e.g., 9.0 ms, probe the Al environments more distant from the Si atoms, i.e., further away from the SiO_x/Al_2O_3 interface and peering deeper into Al_2O_3 and the ALD-grown SiO_x layer (vide infra). The presence of $^{[4]}$Al, $^{[5]}$Al, and $^{[6]}$Al sites, associated with peaks centered at approximately 60, 30, and 10 ppm, respectively, was observed for all tested recoupling times (1.5, 3.0, 6.0, and 9.0 ms) for both Si1- and Si10−Al_2O_{3-600}. However, in both Si1- and Si10−Al_2O_{3-600}, longer recoupling times showed an increasing contribution of $^{[4]}$Al and $^{[5]}$Al sites relative to the spectra acquired with a recoupling time of 1.5 ms. This increase is subtle for Si1−Al_2O_{3-600}, but more clearly observable for Si10−Al_2O_{3-600}. For Si1−Al_2O_{3-600}, this increase in the contribution of $^{[4]}$Al and $^{[5]}$Al sites can be due to probing more distant (from the Si at the interface) surface Al sites, consistent with a submonolayer Si coverage in this material. As $^{[6]}Al_{(Al)}$ surface sites in γ-Al_2O_{3-600} are OH-terminated, while $^{[4]}Al_{(Al)}$ and $^{[5]}Al_{(Al)}$ surface sites can either be OH-terminated or OH-free,[10,68] we hypothesize that the grafting of BDEAS onto aluminols and subsequent calcination generate $^{[4,5,6]}Al_{(Al,Si)}$ sites from $^{[4,5,6]}Al_{(Al)}$−OH sites. At the same time, OH-free $^{[4]}Al_{(Al)}$ and $^{[5]}Al_{(Al)}$ remain mostly unmodified by ALD, and it is those sites that are probed at higher recoupling times. In contrast, for Si10−Al_2O_{3-600}, the observed increase in the contribution of $^{[4]}$Al and $^{[5]}$Al sites, as

https://doi.org/10.1021/acs.chemmater.5c01832
Chem. Mater. 2025, 37, 7974−7986

well as the increase in signal-to-noise ratio, can be explained by the diffusion of Al^{3+} into the deposited layer of SiO_x, forming ASA. The relative intensity of $^{[6]}$Al sites decreases for a longer recoupling time in Si10−Al_2O_{3-600} because such $^{[6]}$Al sites are located in the vicinity of Si sites, mainly at the SiO_x/Al_2O_3 interface.

The presence of $^{[5]}$Al sites and the broadening of all peaks differentiate the spectra of Si1- and Si10−Al_2O_{3-600} from that of γ-Al_2O_{3-600} (obtained via a direct detection measurement from the bulk of Si1- and Si10−Al_2O_{3-600}), indicating an appreciably larger distribution of local Al environments at or near the SiO_x/Al_2O_3 interface in the Si-containing materials. Simulating experiments with a recoupling time of 6.0 ms provided a relative ratio of signal intensities around 69, 37, and 12 ppm, assigned to $^{[4]}$Al:$^{[5]}$Al:$^{[6]}$Al sites in Si1- and Si10−Al_2O_{3-600}, as 58:24:18 and 69:13:18, respectively (Figure S15). These results suggest that additional ALD cycles reorganize the (near-) surface structure of Si1−Al_2O_{3-600} by increasing the amount of $^{[4]}$Al sites, which correlates with the increasing strength of LAS and BAS with Si loading. The low signal-to-noise (S/N) ratio for the experiments at short recoupling times makes the assessment of the local Al environments at the SiO_x/Al_2O_3 interface challenging. However, the systematically lower S/N ratio for Si1−Al_2O_{3-600} than for Si10−Al_2O_{3-600} at a recoupling time of 1.5 ms suggests that a smaller total amount of Al atoms is located near Si in Si1−Al_2O_{3-600}; an observation that is consistent with a submonolayer coverage of the Al_2O_3 surface by SiO_x in Si1−Al_2O_{3-600} and the diffusion of Al^{3+} into the SiO_x layer in Si10−Al_2O_{3-600}. The diffusion of Si atoms into crystalline Al_2O_3 particles is considered improbable as it is inconsistent with the absence of an appreciable decrease in the relative intensity of $^{[5]}$Al sites with increasing recoupling time for both Si1−Al_2O_{3-600} and Si10−Al_2O_{3-600}. In contrast, the migration of Al^{3+} into the SiO_x layer increases the amount of Si in the vicinity of Al and therefore the signal increases.

It is worth noting that ^{29}Si{^{1}H} DNP SENS mainly probes the outer surface of the deposited silica layer, whereas both the ^{27}Al{^{29}Si} D-HMQC and ^{29}Si{^{27}Al} D-RINEPT CPMG experiments are more selective to the SiO_x/Al_2O_3 interface.[24,69] The ^{29}Si spectra of Si1−Al_2O_{3-600} under various experimental conditions (^{27}Al{^{29}Si} D-HMQC, ^{29}Si{^{1}H} DNP SENS and ^{29}Si{^{27}Al} D-RINEPT CPMG) are remarkably similar (Figure 6c). The similarity of the Si1−Al_2O_{3-600} spectra obtained using these three methods indicates that one ALD cycle deposits a thin silica film in which all Si sites are in contact with the Al_2O_3 surface and the radical-containing impregnated DNP solution, which fills the particles' intergrain space. This is in contrast with the result obtained for Si10−Al_2O_{3-600}, for which the ^{29}Si{^{1}H} DNP SENS spectrum features higher relative intensity in the range between −100 ppm and ca. −110 ppm compared to the ^{27}Al{^{29}Si} D-HMQC spectrum (Figure 6d). The peaks at −100 ppm and −110 ppm are associated with extended siloxane networks (Si−O−Si species) at the outer surface of the ALD-deposited layer, and mainly assigned to $(AlO)_1Si(OSi)_3$ and $Si(OSi)_4$ sites, respectively.[70] At the same time, the indirect spectrum extracted from the 2D ^{27}Al{^{29}Si} D-HMQC data of Si10−Al_2O_{3-600} evidences relatively high signal intensities around −85 ppm, corresponding to $(AlO)_{(4-p)}Si(OSi)_p$ or $(AlO)_{(3-p)}SiOH(OSi)_p$.[70] The presence of the latter sites in Si10−Al_2O_{3-600} is also evidenced by ^{29}Si{^{27}Al} D-RINEPT, as the intensity around −85 ppm in the ^{29}Si{^{27}Al} D-RINEPT spectrum is intermediate between the intensities at −85 ppm of the ^{27}Al{^{29}Si} D-HMQC and ^{29}Si{^{1}H} DNP SENS spectra, explained by the used CPMG acquisition scheme for signal-to-noise enhancement, which increases to a higher extent intensities of sites with long transverse relaxation times such as $Si(OSi)_4$ relative to silanol sites.[71]

Two-dimensional Al/Si correlations presented in Figure 6e,f reveal a more disordered nature of Si sites in Si10−Al_2O_{3-600} than in Si1−Al_2O_{3-600}, as the former contains a broader range of silicon environments, spreading the 2D line shapes along the ^{29}Si dimension. For Si1−Al_2O_{3-600}, there is no preference of Si to a specific Al coordination (i.e., $^{[4]}$Al, $^{[5]}$Al, or $^{[6]}$Al) in $(AlO)_{(4-p)}Si(OSi)_p$ or $(AlO)_{(3-p)}SiOH(OSi)_p$; in other words, all Si sites are close to Al sites in all three coordination geometries. This does not appear to be the case for Si10−Al_2O_{3-600} since the maxima of the 2D lines are not at the same position on the ^{29}Si dimension, yet the low S/N of those 2D lines prevents a more detailed analysis.

■ DISCUSSION

In a previous report, it was shown that the deposition of one ALD cycle of trimethylaluminum (3.4 wt % Al deposited) onto amorphous dehydroxylated silica generates a higher amount of strong BAS than after 5 or 10 ALD cycles, i.e., strong BAS reside primarily at the AlO_x/SiO_2 interface rather than on the subsequently grown AlO_x layers.[24] In contrast, the present results reveal that the deposition of SiO_x by ALD onto dehydroxylated crystalline alumina requires 5−10 ALD cycles (5.9−9.9 wt % Si) for an appreciable amount of strong BAS to form. The relatively high amount of deposited Si required to yield strong BAS is likely related to the crystallinity of alumina, as similar findings have been reported when comparing materials (after calcination) obtained by grafting molecular Al precursors onto amorphous silica and Si precursors onto crystalline alumina.[25] Specifically, it was found that grafting Al precursors onto silica, followed by calcination, preferentially formed $^{[4]}$Al−O−$^{[4]}$Si linkages (a $^{[4]}Al_{(Si)}$ site), which has been linked to strong BAS.[25] It has been argued that the higher covalency of the Al−O−Si bonding relative to the more ionic Al−O−Al bonding causes an increase in the relative ratio of $^{[4]}$Al/$^{[6]}$Al sites, as Al sites prefer a $^{[4]}$Al coordination geometry in more covalent environments.[25] Our work estimates the relative ratio of $^{[4]}$Al:$^{[5]}$:Al:$^{[6]}$Al sites in the vicinity of Si atoms in Si1- and Si10−Al_2O_{3-600} as 58:24:18 and 69:13:18, respectively, implying that a more significant amount of deposited Si increases the relative fraction of $^{[4]}$Al sites around Si, which is associated with the emergence of strong BAS and an increase in strength of LAS.[21] Considering that TEM reveals a homogeneous, several nanometers thin overlayer of SiO_x on Si10−Al_2O_3, and at the same time, there is an appreciable amount of strong BAS together with strong and medium LAS in this material, and no weak LAS of alumina, the diffusion of Al^{3+} from the SiO_x/Al_2O_3 interface into the surface (layer) of the deposited SiO_x is very likely.

Interestingly, in both Si1 and Si10−Al_2O_{3-600}, the intensity of $^{[6]}$Al sites around Si atoms in the ^{27}Al{^{29}Si} $SR4_1^2$ D-HMQC spectrum is higher than that of the $^{[4]}$Al and $^{[5]}$Al sites when using a short recoupling time of 1.5 ms. This result indicates that also for Si10−Al_2O_{3-600}, the interface between SiO_x and Al_2O_3 contributes most to the Al signal intensity, and the amount of isolated $^{[4]}Al_{(Si)}$ sites within the ALD-grown layer and on its surface is relatively low. This is indeed consistent with the largely decreased intensity of Py−LAS bands in the

https://doi.org/10.1021/acs.chemmater.5c01832
Chem. Mater. 2025, 37, 7974−7986

Scheme 1. Summary of Key Structural and Surface Properties Distinguishing Al_2O_{3-600} and Si1−Al_2O_{3-600} from Si5- and Si10−Al_2O_{3-600} in Methanol Dehydration[a]

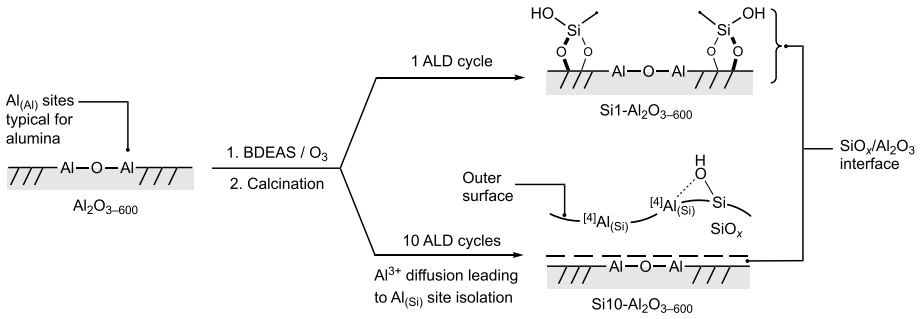

Catalyst	θ(SiO_x)	X(CH_3OH)	S(DME)	Main LAS
Al_2O_3	none	high	low	$Al_{(Al)}$
Si1-Al_2O_3	sub-ML	high	medium	$Al_{(Al)}$
Si10-Al_2O_3	several-ML	medium	high	$Al_{(Si)}$

* θ, X, and S stand for coverage, conversion, and selectivity, respectively

[a]For Si1−Al_2O_{3-600}, the SiO_x/Al_2O_3 interface is the particles' outer surface.

Scheme 2. Proposed Mechanisms for the Methanol-to-DME Dehydration on (a) $Al_{(Al)}$ Weak LAS of Al_2O_{3-600} and Si1−Al_2O_{3-600}, (b) Strong BAS of Si5- and Si10−Al_2O_{3-600}, and (c) Key Steps for the DME Decomposition to Methane on the $Al_{(Al)}$ Site of Al_2O_3

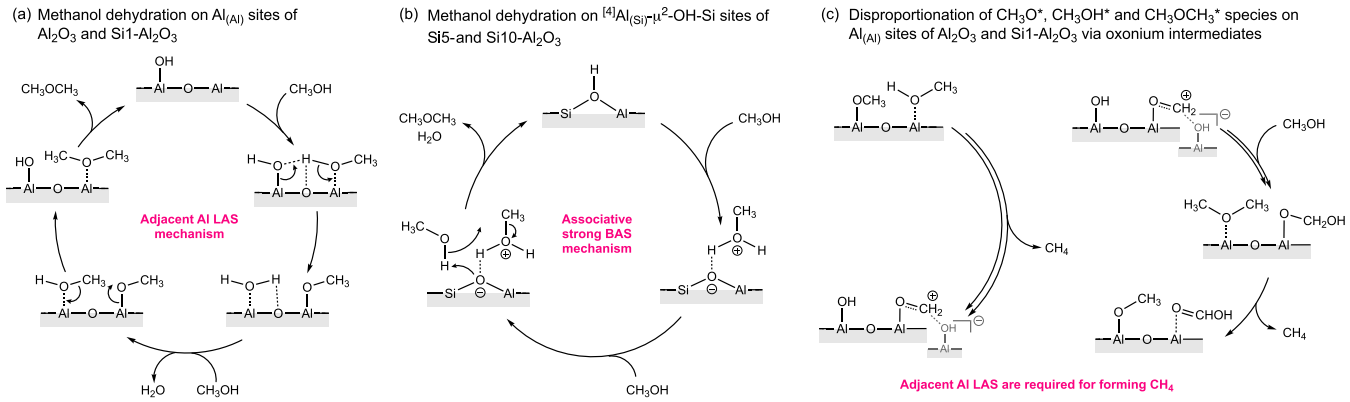

Py-FTIR experiment on Si10−Al_2O_{3-600} compared to Si1−Al_2O_{3-600}. Noteworthy, the presence of a submonolayer SiO_x in Si1−Al_2O_{3-600} resulted in the increase of the strength of all LAS (i.e., weak, medium, and strong LAS of alumina). Interestingly, ^{15}N-Py DNP SENS distinguishes two strong BAS in Si5- and Si10−Al_2O_{3-600} materials. These two Brønsted sites may be due to pseudobridging silanols and zeolite-like BAS, as reported for ASA.[28,29] The proposed processes prevailing in the ALD-prepared materials and key experimental observations are summarized in Scheme 1.

Next, we aim to correlate insights into the local structure of Si and Al sites and surface acidity with methanol-to-DME conversion at 250 °C and DME selectivity at 450 °C. Alcohol dehydration on γ-Al_2O_3 has been reported to proceed on a Lewis acid − Lewis base pair.[72,73] More specifically, an Al−O−Al(OH) site has been proposed for the dehydration reaction, which transforms adsorbed methanol into an OCH_3* species and, through interaction with a second methanol molecule, to DME.[74] This mechanism is presented in Scheme 2a. Notably, the pathway requires an $Al_{(Al)}$ site to activate the second methanol molecule on the neighboring (to the formed OCH_3* species) LAS, facilitating the methoxy group attack and leading to the formation of DME. However, diverging results have been reported regarding the role of the strength of the specific Lewis acid sites. An early report on 1-butanol dehydration on Al_2O_3 suggested weak and mild LAS as the active dehydration sites,[75] which was subsequently confirmed for the conversion of methanol-to-DME on γ-Al_2O_3.[76] That being said, strong LAS on silica−alumina catalysts and strong BAS on zeolite catalysts have also been discussed as the active centers for ethanol and methanol dehydration, respectively.[74,77]

Considering these previous reports, the higher methanol conversion at 250 °C on Al_2O_{3-600} and Si1−Al_2O_{3-600} and the lower conversion on Si5 and Si10−Al_2O_3 catalysts correlates with the amount of $Al_{(Al)}$ LAS, i.e., the proposed active sites for the mechanism presented in Scheme 2a. Both the total amount of LAS and the amount of $Al_{(Al)}$ LAS decrease with increasing Si loading, leading to a simultaneous increase in strong BAS. While an increasing quantity of Si deposited leads to a higher relative fraction of $^{[4]}Al_{(Si)}$ sites, which are stronger LAS than those in Al_2O_{3-600}, there is a concurrent decrease in the total amount of LAS due to the coverage of the Al^{3+} sites of alumina with a SiO_x layer that is offset only partially by the diffusion of Al^{3+} into the SiO_x overlayer in Si5- and Si10−Al_2O_{3-600}. The presence of weak LAS in Al_2O_{3-600} and Si1−Al_2O_{3-600}, ascribed to $^{[5]}Al_{(Al)}$ sites of alumina,[25,54] indeed correlates with the higher methanol conversion of Al_2O_{3-600} and Si1−Al_2O_{3-600} at 250 °C, while the lack of such weak LAS and isolation of Al^{3+} sites in Si5- and Si10−Al_2O_{3-600} correlates with their lower methanol conversion at 250 °C. As weak $Al_{(Al)}$ LAS are not found in Si5- and Si10−Al_2O_{3-600}, it is conceivable that the latter two catalysts convert methanol to DME via a strong BAS mechanism presented in Scheme 2b. Furthermore, the structural differences as a function of Si deposition as discussed above, also explain the trend in DME decomposition at 450 °C. As the formation of DME from methanol, also the decomposition of DME has been suggested to involve two adjacent Al atoms, i.e., $Al_{(Al)}$ sites.[45] Consistent

https://doi.org/10.1021/acs.chemmater.5c01832
Chem. Mater. 2025, 37, 7974−7986

with this hypothesis, in our work, the weak or medium strength $Al_{(Al)}$ LAS of Al_2O_{3-600} and Si1−Al_2O_{3-600} were found to decompose DME to CH_4 through the steps depicted in Scheme 2c. At the same time, strong LAS such as $^{[4]}Al_{(Si)}$ in Si5- and Si10−Al_2O_{3-600} or BAS do not drive this reaction due to the lack of two adjacent Al atoms, confirming site isolation of Al^{3+} sites in these materials.

■ CONCLUSION

This study provides an atomic-scale characterization of ALD-derived silica layers on partially dehydroxylated Al_2O_3, offering insight into the local structures at the interfacial sites that control surface acidity and the catalytic activity of the materials in methanol dehydration. Specifically, it was found that $Al_{(Al)}$ Lewis sites drive methanol dehydration to DME at 250 °C in Al_2O_{3-600} and Si1−Al_2O_{3-600}. Covering such $Al_{(Al)}$ sites with silica overlayers and the diffusing of Al^{3+} within the grown layer creates strong LAS and BAS containing $^{[4]}Al_{(Si)}$ sites. Such isolated $^{[4]}Al_{(Si)}$ surface sites are observed in Si5- and Si10−Al_2O_{3-600} but are largely absent in Si1−Al_2O_{3-600}, i.e., at the SiO_x/Al_2O_3 interface. The isolated $^{[4]}Al_{(Si)}$ LAS are less active in methanol dehydration to DME at 250 °C relative to the $Al_{(Al)}$ sites of alumina. However, $^{[4]}Al_{(Si)}$ sites, unlike $Al_{(Al)}$ sites, do not readily decompose DME to CH_4 at 450 °C. Our structural analysis reveals the evolution of surface acidity with increasing quantities of SiO_x being deposited by ALD, underscoring the critical role of such silica−alumina overlayers in determining the catalytic properties in methanol dehydration to DME and the decomposition of DME to methane. This insight enhances our atomic-level understanding of surface and interfacial properties, leading ultimately to the design of more efficient heterogeneous catalysts.

■ ASSOCIATED CONTENT

Supporting Information

The Supporting Information is available free of charge at https://pubs.acs.org/doi/10.1021/acs.chemmater.5c01832.

Experimental procedures; additional data analyses; N_2 adsorption and desorption isotherms; IR spectra; XRD patterns; TEM and HAADF-STEM images; EDX maps; product selectivity plot; NH_3 TPD deconvolution plots; CO−DRIFTS spectra; simulations of $^{27}Al\{^{29}Si\}$ $SR4_1^2$ D-HMQC spectra; Raman spectra; tabulated results of Si loading, BET surface area, pore volume, and pore diameter; fitting parameters of the ^{29}Si and ^{15}N DNP SENS data; results of the catalytic tests; and quantification of Py-FTIR spectra and NH_3 TPD (PDF)

■ AUTHOR INFORMATION

Corresponding Authors

Pierre Florian − *CNRS, CEMHTI UPR3079, Université d'Orléans, 45071 Orléans, France;* orcid.org/0000-0003-4306-0815; Email: pierre.florian@cnrs-orleans.fr

Christoph R. Müller − *Department of Mechanical and Process Engineering, ETH Zürich, CH-8092 Zürich, Switzerland;* orcid.org/0000-0003-2234-6902; Email: muelchri@ethz.ch

Alexey Fedorov − *Department of Mechanical and Process Engineering, ETH Zürich, CH-8092 Zürich, Switzerland;* orcid.org/0000-0001-9814-6726; Email: fedoroal@ethz.ch

Authors

Melis Yarar − *Department of Mechanical and Process Engineering, ETH Zürich, CH-8092 Zürich, Switzerland;* orcid.org/0000-0003-1936-7905

Zixuan Chen − *Department of Mechanical and Process Engineering, ETH Zürich, CH-8092 Zürich, Switzerland;* orcid.org/0000-0002-3882-3016

Diana Piankova − *Department of Mechanical and Process Engineering, ETH Zürich, CH-8092 Zürich, Switzerland;* orcid.org/0000-0002-3098-6822

Matthias Becker − *Department of Mechanical and Process Engineering, ETH Zürich, CH-8092 Zürich, Switzerland;* orcid.org/0009-0001-2040-6783

Alexander V. Yakimov − *Department of Chemistry and Applied Biosciences, ETH Zürich, CH-8093 Zürich, Switzerland;* orcid.org/0000-0002-8624-1002

Christophe Copéret − *Department of Chemistry and Applied Biosciences, ETH Zürich, CH-8093 Zürich, Switzerland;* orcid.org/0000-0001-9660-3890

Complete contact information is available at: https://pubs.acs.org/10.1021/acs.chemmater.5c01832

Author Contributions

M.Y. and A.F. conceived the research project and designed the experiments. M.Y. and Z.C. synthesized the materials. M.Y. characterized the materials, performed the catalytic tests, and analyzed the data. A.V.Y. supervised DNP SENS experiments and data analysis. M.B. and A.V.Y. conducted ^{29}Si and ^{15}N DNP SENS experiments. D.P. acquired the TEM data and performed data analysis. P.F. designed and conducted $^{27}Al\{^{29}Si\}$ and $^{29}Si\{^{27}Al\}$ NMR experiments and analyzed the data. C.R.M. and C.C. acquired funding. M.Y., P.F., and A.F. wrote the first draft, which was reviewed and edited by all authors. All authors contributed to the discussion and approved the final manuscript.

Notes

The authors declare no competing financial interest.

■ ACKNOWLEDGMENTS

Clariant supported this work through a doctoral fellowship to M.Y. ETH Zürich supported this work through a doctoral fellowship to Z.C. (ETH-40 17-2). SNSF supported this work through a postdoctoral fellowship to D.P. (TMPFP2_224646). We are grateful to the Scientific Centre for Optical and Electron Microscopy (ScopeM, ETH Zürich) for providing access to electron microscopy facilities. We thank the Pan-European Solid-State NMR Infrastructure for Chemistry-Enabling Access (PANACEA program, funding from the European Union's Horizon 2020 research and innovation program under grant agreement 101008500) and the ETH+ project SynMatLab (funding from ETH Zurich) for the measurement time and expertise. Dr. Paula M. Abdala (ETH Zürich) is thanked for regular discussions.

■ REFERENCES

(1) Busca, G. Acid Catalysts in Industrial Hydrocarbon Chemistry. *Chem. Rev.* **2007**, *107*, 5366−5410.

(2) Corma, A. Inorganic Solid Acids and Their Use in Acid-Catalyzed Hydrocarbon Reactions. *Chem. Rev.* **1995**, *95*, 559−614.

(3) Busca, G. Catalytic Materials Based on Silica and Alumina: Structural Features and Generation of Surface Acidity. *Prog. Mater. Sci.* **2019**, *104*, 215−249.

(4) Chizallet, C. Toward the Atomic Scale Simulation of Intricate Acidic Aluminosilicate Catalysts. *ACS Catal.* **2020**, *10*, 5579−5601.
(5) Copéret, C. C.; Comas-Vives, A.; Conley, M. P.; Estes, D. P.; Fedorov, A.; Mougel, V.; Nagae, H.; Núñez-Zarur, F. N.; Zhizhko, P. A. Surface Organometallic and Coordination Chemistry toward Single-Site Heterogeneous Catalysts: Strategies, Methods, Structures, and Activities. *Chem. Rev.* **2016**, *116*, 323−421.
(6) Caillot, M.; Chaumonnot, A.; Digne, M.; Bokhoven, J. A. V. Quantification of Brønsted Acid Sites of Grafted Amorphous Silica−Alumina Compounds and Their Turnover Frequency in m-Xylene Isomerization. *ChemCatChem.* **2013**, *5*, 3644−3656.
(7) Yi, X.; Liu, K.; Chen, W.; Li, J.; Xu, S.; Li, C.; Xiao, Y.; Liu, H.; Guo, X.; Liu, S. B.; Zheng, A. Origin and Structural Characteristics of Tri-Coordinated Extra-Framework Aluminum Species in Dealuminated Zeolites. *J. Am. Chem. Soc.* **2018**, *140*, 10764−10774.
(8) Digne, M.; Sautet, P.; Raybaud, P.; Euzen, P.; Toulhoat, H. Use of DFT to Achieve a Rational Understanding of Acid-Basic Properties of γ-Alumina Surfaces. *J. Catal.* **2004**, *226*, 54−68.
(9) Wischert, R.; Copéret, C.; Delbecq, F.; Sautet, P. Dinitrogen: A Selective Probe for Tri-Coordinate Al "Defect" Sites on Alumina. *Chem. Commun.* **2011**, *47*, 4890−4892.
(10) Wischert, R.; Laurent, P.; Copéret, C.; Delbecq, F.; Sautet, P. γ-Alumina: The Essential and Unexpected Role of Water for the Structure, Stability, and Reactivity of "Defect" Sites. *J. Am. Chem. Soc.* **2012**, *134*, 14430−14449.
(11) Samudrala, K. K.; Huynh, W.; Dorn, R. W.; Rossini, A. J.; Conley, M. P. Formation of a Strong Heterogeneous Aluminum Lewis Acid on Silica. *Angew. Chem., Int. Ed.* **2022**, *61*, No. e202205745.
(12) Chizallet, C.; Raybaud, P. Acidity of Amorphous Silica-Alumina: From Coordination Promotion of Lewis Sites to Proton Transfer. *ChemPhysChem* **2010**, *11*, 105−108.
(13) Crépeau, G.; Montouillout, V.; Vimont, A.; Mariey, L.; Cseri, T.; Maugé, F. Nature, Structure and Strength of the Acidic Sites of Amorphous Silica Alumina: An IR and NMR Study. *J. Phys. Chem. B* **2006**, *110*, 15172−15185.
(14) Rivera-Barrera, D.; Guzman, A.; Ramirez, I.; Molina, V. D. Effect of Si/Al Ratio, Calcination Temperature and Post-Synthesis Phosphorus Modification on the Textural, Structural, Acidic, and Catalytic Properties of Amorphous Silica-Alumina Prepared by Deposition Methods. *J. Phys. Chem. Solids* **2024**, No. 112403.
(15) Huang, J.; Van Vegten, N.; Jiang, Y.; Hunger, M.; Baiker, A. Increasing the Brønsted Acidity of Flame-Derived Silica/Alumina up to Zeolitic Strength. *Angew. Chem., Int. Ed.* **2010**, *49*, 7776−7781.
(16) Trombetta, M.; Busca, G.; Rossini, S.; Piccoli, V.; Cornaro, U.; Guercio, A.; Catani, R.; Willey, R. J. FT-IR Studies on Light Olefin Skeletal Isomerization Catalysis III. Surface Acidity and Activity of Amorphous and Crystalline Catalysts Belonging to the SiO_2-Al_2O_3 System. *J. Catal.* **1998**, *179*, 581−596.
(17) Chizallet, C.; Raybaud, P. Pseudo-Bridging Silanols as Versatile Brønsted Acid Sites of Amorphous Aluminosilicate Surfaces. *Angew. Chem., Int. Ed.* **2009**, *48*, 2891−2893.
(18) Larmier, K.; Chizallet, C.; Maury, S.; Cadran, N.; Abboud, J.; Lamic-Humblot, A. F.; Marceau, E.; Lauron-Pernot, H. Isopropanol Dehydration on Amorphous Silica−Alumina: Synergy of Brønsted and Lewis Acidities at Pseudo-Bridging Silanols. *Angew. Chem., Int. Ed.* **2017**, *56*, 230−234.
(19) Perras, F. A.; Wang, Z.; Kobayashi, T.; Baiker, A.; Huang, J.; Pruski, M. Shedding Light on the Atomic-Scale Structure of Amorphous Silica-Alumina and Its Brønsted Acid Sites. *Phys. Chem. Chem. Phys.* **2019**, *21*, 19529−19537.
(20) Wang, Z.; Li, T.; Jiang, Y.; Lafon, O.; Liu, Z.; Trébosc, J.; Baiker, A.; Amoureux, J. P.; Huang, J. Acidity Enhancement through Synergy of Penta- and Tetra-Coordinated Aluminum Species in Amorphous Silica Networks. *Nat. Commun.* **2020**, *11*, 225.
(21) Wang, Z.; Jiang, Y.; Baiker, A.; Huang, J. Pentacoordinated Aluminum Species: New Frontier for Tailoring Acidity-Enhanced Silica-Alumina Catalysts. *Acc. Chem. Res.* **2020**, *53*, 2648−2658.
(22) Wang, Z.; Jiang, Y.; Lafon, O.; Trébosc, J.; Duk Kim, K.; Stampfl, C.; Baiker, A.; Amoureux, J. P.; Huang, J. Brønsted Acid Sites Based on Penta-Coordinated Aluminum Species. *Nat. Commun.* **2016**, *7*, 13820.
(23) Caillot, M.; Chaumonnot, A.; Digne, M.; Van Bokhoven, J. A. The Variety of Brønsted Acid Sites in Amorphous Aluminosilicates and Zeolites. *J. Catal.* **2014**, *316*, 47−56.
(24) Kaushik, M.; Leroy, C.; Chen, Z.; Gajan, D.; Willinger, E.; Müller, R. C.; Fayon, F.; Massiot, D.; Fedorov, A.; Copéret, C.; Lesage, A.; Florian, P. Atomic-Scale Structure and Its Impact on Chemical Properties of Aluminum Oxide Layers Prepared by Atomic Layer Deposition on Silica. *Chem. Mater.* **2021**, *33*, 3335−3348.
(25) Valla, M.; Rossini, J. A.; Caillot, M.; Chizallet, C.; Raybaud, P.; Digne, M.; Chaumonnot, A.; Lesage, A.; Emsley, L.; van Bokhoven, A. J.; Copéret, C. Atomic Description of the Interface between Silica and Alumina in Aluminosilicates through Dynamic Nuclear Polarization Surface-Enhanced NMR Spectroscopy and First-Principles Calculations. *J. Am. Chem. Soc.* **2015**, *137*, 10710−10719.
(26) Ardagh, M. A.; Bo, Z.; Nauert, S. L.; Notestein, J. M. Depositing SiO_2 on Al_2O_3: A Route to Tunable Brønsted Acid Catalysts. *ACS Catal.* **2016**, *6*, 6156−6164.
(27) Hensen, E. J. M.; Poduval, D. G.; Degirmenci, V.; Ligthart, D. A. J. M.; Chen, W.; Maugé, F.; Rigutto, M. S.; Van Veen, J. A. R. Acidity Characterization of Amorphous Silica-Alumina. *J. Phys. Chem. C* **2012**, *116*, 21416−21429.
(28) Wang, Z.; Chen, K.; Jiang, Y.; Trébosc, J.; Yang, W.; Amoureux, J. P.; Hung, I.; Gan, Z.; Baiker, A.; Lafon, O.; Huang, J. Revealing Brønsted Acidic Bridging SiOHAl Groups on Amorphous Silica-Alumina by Ultrahigh Field Solid-State NMR. *J. Phys. Chem. Lett.* **2021**, *12*, 11563−11572.
(29) Salvia, W. S.; Zhao, T. Y.; Chatterjee, P.; Huang, W.; Perras, F. A. Are the Brønsted Acid Sites in Amorphous Silica-Alumina Bridging? *Chem. Commun.* **2023**, *59*, 13962−13965.
(30) Kobayashi, T.; Perras, F. A.; Slowing, I. I.; Sadow, A. D.; Pruski, M. Dynamic Nuclear Polarization Solid-State NMR in Heterogeneous Catalysis Research. *ACS Catal.* **2015**, *5*, 7055−7062.
(31) Rankin, A. G. M.; Webb, P. B.; Dawson, D. M.; Viger-Gravel, J.; Walder, B. J.; Emsley, L.; Ashbrook, S. E. Determining the Surface Structure of Silicated Alumina Catalysts via Isotopic Enrichment and Dynamic Nuclear Polarization Surface-Enhanced NMR Spectroscopy. *J. Phys. Chem. C* **2017**, *121*, 22977−22984.
(32) Chen, Z.; Serykh, A. I.; Kierzkowska, A.; Gajan, D.; Docherty, S. R.; Yakimov, A. V.; Abdala, P. M.; Copéret, C.; Florian, P.; Fedorov, A.; Müller, C. R. Reversible Transformation of Sub-Nanometer Ga-Based Clusters to Isolated $^{[4]}Ga_{(4Si)}$ Sites Creates Active Centers for Propane Dehydrogenation. *Catal. Sci. Technol.* **2024**, *14*, 379−390.
(33) Fărcaşiu, D.; Leu, R.; Corma, A. Evaluation of Accessible Acid Sites on Solids by ^{15}N NMR Spectroscopy with Di-Tert-Butylpyridine as Base. *J. Phys. Chem. B* **2002**, *106*, 928−932.
(34) Chen, Z.; Zimmerli, N. K.; Zubair, M.; Yakimov, A. V.; Björgvinsdóttir, S.; Alaniva, N.; Willinger, E.; Barnes, A. B.; Bedford, N. M.; Copéret, C.; Florian, P.; Abdala, P. M.; Fedorov, A.; Müller, C. R. Nature of GaO_x Shells Grown on Silica by Atomic Layer Deposition. *Chem. Mater.* **2023**, *35*, 7475−7490.
(35) Coumans, F.; Mezari, B.; Zuidema, N.; Heinrichs, J. M. J. J.; Hensen, E. J. M. Isolating Al Surface Sites in Amorphous Silica-Alumina by Homogeneous Deposition of Al^{3+} on SiO_2 Nanoparticles. *ACS Appl. Nano Mater.* **2024**, *7*, 25524−25534.
(36) Busca, G. Silica-Alumina Catalytic Materials: A Critical Review. *Catal. Today* **2020**, *357*, 621−629.
(37) Mouat, A. R.; Kobayashi, T.; Pruski, M.; Marks, T. J.; Stair, P. C. Direct Spectroscopic Evidence for Isolated Silanols in SiO_x/Al_2O_3 and Their Formation Mechanism. *J. Phys. Chem. C* **2017**, *121*, 6060−6064.
(38) Mouat, A. R.; George, C.; Kobayashi, T.; Pruski, M.; Van Duyne, R. P.; Marks, T. J.; Stair, P. C. Highly Dispersed SiO_x/Al_2O_3 Catalysts Illuminate the Reactivity of Isolated Silanol Sites. *Angew. Chem., Int. Ed.* **2015**, *54*, 13346−13351.

(39) Zhang, B.; Qin, Y. Interface Tailoring of Heterogeneous Catalysts by Atomic Layer Deposition. *ACS Catal.* **2018**, *8*, 10064−10081.
(40) Barry, S. T.; Teplyakov, A. V.; Zaera, F. The Chemistry of Inorganic Precursors during the Chemical Deposition of Films on Solid Surfaces. *Acc. Chem. Res.* **2018**, *51*, 800−809.
(41) Puurunen, R. L. Surface Chemistry of Atomic Layer Deposition: A Case Study for the Trimethylaluminum/Water Process. *J. Appl. Phys.* **2005**, *97*, 121301.
(42) Mione, M. A.; Vandalon, V.; Mameli, A.; Kessels, W. M. M.; Roozeboom, F. Atmospheric-Pressure Plasma-Enhanced Spatial ALD of SiO_2 Studied by Gas-Phase Infrared and Optical Emission Spectroscopy. *J. Phys. Chem. C* **2021**, *125*, 24945−24957.
(43) Kazansky, V. B. The Study of Bronsted and Lewis Acidity of Decationized and Dealuminated Zeolites by IR-Diffuse Reflectance Spectroscopy and Quantum Chemistry. *Stud. Surf. Sci. Catal.* **1984**, *18*, 61−75.
(44) Akarmazyan, S. S.; Panagiotopoulou, P.; Kambolis, A.; Papadopoulou, C.; Kondarides, D. I. Methanol Dehydration to Dimethylether over Al_2O_3 Catalysts. *Appl. Catal. B: Environ.* **2014**, *145*, 136−148.
(45) Comas-Vives, A.; Valla, M.; Copéret, C.; Sautet, P. Cooperativity between Al Sites Promotes Hydrogen Transfer and Carbon-Carbon Bond Formation upon Dimethyl Ether Activation on Alumina. *ACS Cent. Sci.* **2015**, *1*, 313−319.
(46) Sanchez-Sanchez, M. C.; Yerga, R. M. N.; Kondarides, D. I.; Verykios, X. E.; Fierro, J. L. G. Mechanistic Aspects of the Ethanol Steam Reforming Reaction for Hydrogen Production on Pt, Ni, and PtNi Catalysts Supported on γ-Al_2O_3. *J. Phys. Chem. C* **2010**, *114*, 3873−3882.
(47) Lafer, L. I.; Yakerson, V. I.; Rubinshtein, A. M. Infrared Spectra of Catalysts and Adsorbed Molecules Communication 5. Methanol on the Surface of Aluminum Oxide. *Russ. Chem. Bull.* **1967**, *16*, 2312−2318.
(48) Barzetti, T.; Selli, E.; Moscotti, D.; Forni, L. Pyridine and Ammonia as Probes for FTIR Analysis of Solid Acid Catalysts. *J. Chem. Soc., Faraday Trans.* **1996**, *92*, 1401−1407.
(49) Sandoval-Díaz, L. E.; González-Amaya, J. A.; Trujillo, C. A. General Aspects of Zeolite Acidity Characterization. *Microporous Mesoporous Mater.* **2015**, *215*, 229−243.
(50) Kiatphuengporn, S.; Junkaew, A.; Luadthong, C.; Thongratkaew, S.; Yimsukanan, C.; Songtawee, S.; Butburee, T.; Khemthong, P.; Namuangruk, S.; Kunaseth, M.; Faungnawakij, K. Roles of Acidic Sites in Alumina Catalysts for Efficient D-Xylose Conversion to Lactic Acid. *Green Chem.* **2020**, *22*, 8572−8583.
(51) Morterra, C.; Magnacca, G. A Case Study: Surface Chemistry and Surface Structure of Catalytic Aluminas, as Studied by Vibrational Spectroscopy of Adsorbed Species. *Catal. Today* **1996**, *27*, 497−532.
(52) Emeis, C. A. Determination of Integrated Molar Extinction Coefficients for Infrared Absorption Bands of Pyridine Adsorbed on Solid Acid Catalysts. *J. Catal.* **1993**, *141*, 347−354.
(53) Zholobenko, V.; Freitas, C.; Jendrlin, M.; Bazin, P.; Travert, A.; Thibault-Starzyk, F. Probing the Acid Sites of Zeolites with Pyridine: Quantitative AGIR Measurements of the Molar Absorption Coefficients. *J. Catal.* **2020**, *385*, 52−60.
(54) Moroz, I. B.; Larmier, K.; Liao, W. C.; Copéret, C. Discerning γ-Alumina Surface Sites with Nitrogen-15 Dynamic Nuclear Polarization Surface Enhanced NMR Spectroscopy of Adsorbed Pyridine. *J. Phys. Chem. C* **2018**, *122*, 10871−10882.
(55) Gunther, W. R.; Michaelis, V. K.; Griffin, R. G.; Roman-Leshkov, Y. Interrogating the Lewis Acidity of Metal Sites in Beta Zeolites with ^{15}N Pyridine Adsorption Coupled with MAS NMR Spectroscopy. *J. Phys. Chem. C* **2016**, *120*, 28533−28544.
(56) Castro-Fernández, P.; Kaushik, M.; Wang, Z.; Mance, D.; Kountoupi, E.; Willinger, E.; Abdala, P. M.; Copéret, C.; Lesage, A.; Fedorov, A.; Müller, C. R. Uncovering Selective and Active Ga Surface Sites in Gallia-Alumina Mixed-Oxide Propane Dehydrogenation Catalysts by Dynamic Nuclear Polarization Surface Enhanced NMR Spectroscopy. *Chem. Sci.* **2021**, *12*, 15273−15283.
(57) Castro-Fernández, P.; Mance, D.; Liu, C.; Moroz, I. B.; Abdala, P. M.; Pidko, E. A.; Copéret, C.; Fedorov, A.; Müller, C. R. Propane Dehydrogenation on Ga_2O_3-Based Catalysts: Contrasting Performance with Coordination Environment and Acidity of Surface Sites. *ACS Catal.* **2021**, *11*, 907−924.
(58) Moroz, I. B.; Lund, A.; Kaushik, M.; Severy, L.; Gajan, D.; Fedorov, A.; Lesage, A.; Copéret, C. Specific Localization of Aluminum Sites Favors Ethene-to-Propene Conversion on (Al)-MCM-41-Supported Ni(II) Single Sites. *ACS Catal.* **2019**, *9*, 7476−7485.
(59) Kustov, L. M.; Kazanskii, V. B.; Beran, S.; Kubelková, L.; Jiru, P. Adsorption of Carbon Monoxide on ZSM-5 Zeolites. Infrared Spectroscopic Study and Quantum-Chemical Calculations. *J. Phys. Chem.* **1987**, *91*, 5247−5251.
(60) Szanyi, J.; Kwak, J. H. Dissecting the Steps of CO_2 Reduction: 1. The Interaction of CO and CO_2 with γ-Al_2O_3: An in Situ FTIR Study. *Phys. Chem. Chem. Phys.* **2014**, *16*, 15117−15125.
(61) Gribov, E. N.; Zavorotynska, O.; Agostini, G.; Vitillo, J. G.; Ricchiardi, G.; Spoto, G.; Zecchina, A. FTIR Spectroscopy and Thermodynamics of CO and H_2 Adsorbed on γ-, δ- and α-Al_2O_3. *Phys. Chem. Chem. Phys.* **2010**, *12*, 6474−6482.
(62) Hensen, E. J. M.; Poduval, D. G.; Magusin, P. C. M. M.; Coumans, A. E.; Van Veen, J. A. R. Formation of Acid Sites in Amorphous Silica-Alumina. *J. Catal.* **2010**, *269*, 201−218.
(63) Delgado, M. R.; Aréan, C. O. Surface Characterization of Gallia-Silica Prepared by a Sol-Gel Method. *J. Mater. Sci. Lett.* **2003**, *22*, 783−785.
(64) Bordiga, S.; Lamberti, C.; Geobaldo, F.; Zecchina, A.; Palomino, G. T.; Areán, C. O. Fourier-Transform Infrared Study of CO Adsorbed at 77 K on H-Mordenite and Alkali-Metal-Exchanged Mordenites. *Langmuir* **1995**, *11*, 527−533.
(65) Lippmaa, E.; Mági, M.; Samoson, A.; Tarmak, M.; Engelhardt, G. Investigation of the Structure of Zeolites by Solid-State High-Resolution ^{29}Si NMR Spectroscopy. *J. Am. Chem. Soc.* **1981**, *103*, 4992−4996.
(66) Engelhardt, G.; Michel, D. *High-Resolution Solid-State NMR of Silicates and Zeolites*; John Wiley and Sons: New York, NY, 1987.
(67) Chen, K.; Gan, Z.; Horstmeier, S.; White, J. L. Distribution of Aluminum Species in Zeolite Catalysts: ^{27}Al NMR of Framework, Partially-Coordinated Framework, and Non-Framework Moieties. *J. Am. Chem. Soc.* **2021**, *143*, 6669−6680.
(68) Ma, Y.; Tang, F.; Liu, Z.; Li, J.; Wang, H.; Wu, F.; Wang, D.; Lu, A. H. A Thermodynamic Model of the Surface Hydroxylation of γ-Al_2O_3. *Phys. Chem. Chem. Phys.* **2024**, *26*, 19543−19553.
(69) Liao, W. C.; Ghaffari, B.; Gordon, C. P.; Xu, J.; Copéret, C. Dynamic Nuclear Polarization Surface Enhanced NMR Spectroscopy (DNP SENS): Principles, Protocols, and Practice. *Curr. Opin. Colloid Interface Sci.* **2018**, *33*, 63−71.
(70) Radeglia, R.; Engelhardt, G. Correlation of Si-O-T (T = Si OR Al) Angles and ^{29}Si NMR Chemical Shifts in Silicates and Aluminosilicates. Interpretation by Semi-Empirical Quantum-Chemical Considerations. *Chem. Phys. Lett.* **1985**, *114*, 28−30.
(71) Larsen, F. H.; Jakobsen, H. J.; Ellis, P. D.; Nielsen, N. C. QCPMG-MAS NMR of Half-Integer Quadrupolar Nuclei. *J. Magn. Reson.* **1998**, *131*, 144−147.
(72) Xu, M.; Lunsford, J. H.; Goodman, D. W.; Bhattacharyya, A. Synthesis of Dimethyl Ether (DME) from Methanol over Solid-Acid Catalysts. *Appl. Catal. A: Gen.* **1997**, *149*, 289−301.
(73) Knözinger, H.; Kochloefl, K.; Meye, W. Kinetics of the Bimolecular Ether Formation from Alcohols over Alumina. *J. Catal.* **1973**, *28*, 69−75.
(74) Chmielarz, L. Dehydration of Methanol to Dimethyl Ether—Current State and Perspectives. *Catalysts* **2024**, *14*, 308.
(75) Pines, H.; Haag, W. O. Alumina: Catalyst and Support. I. Alumina, Its Intrinsic Acidity and Catalytic Activity. *J. Am. Chem. Soc.* **1960**, *82*, 2471−2483.
(76) Mollavali, M.; Yaripour, F.; Atashi, H.; Sahebdelfar, S. Intrinsic Kinetics Study of Dimethyl Ether Synthesis from Methanol on γ-Al_2O_3 Catalysts. *Ind. Eng. Chem. Res.* **2008**, *47*, 3265−3273.

(77) Phung, T. K.; Busca, G. Ethanol Dehydration on Silica-Aluminas: Active Sites and Ethylene/Diethyl Ether Selectivities. *Catal. Commun.* **2015**, *68*, 110−115.

https://doi.org/10.1021/acs.chemmater.5c01832
Chem. Mater. 2025, 37, 7974−7986